Incorporating Histology into a 3D Microscopic Computer Model of Myocardium to Study Propagation at a Cellular Level

Jeroen Stinstra,[1] Rob MacLeod,[2] and Craig Henriquez[3]

[1]Scientific Computing and Imaging Institute, University of Utah, 72S Central Campus Drive, 3750 WEB, Salt Lake City, UT 84112, USA; [2]Scientific Computing and Imaging Institute, Department of Bioengineering, University of Utah, Salt Lake City, UT, USA; and [3]Department of Bioengineering, Duke University, Durham, NC, USA

Associate Editor Peter E. McHugh oversaw the review of this article.

Abstract—We introduce a 3D model of cardiac tissue to study at a microscopic level the relationship between tissue morphology and propagation of depolarization. Unlike the classical bidomain approach, in which tissue properties are described by the apparent conductivity of the tissue, in this "microdomain" approach, we included histology by modeling the actual shape of the intracellular and extracellular spaces that contain spatially distributed gap-junctions and membranes. The histological model of the tissue was generated by a computer algorithm that can be tuned to model different histological changes. For healthy tissue, the model predicted a realistic conduction velocity of 0.42 m/s based solely on the parameters derived from histology. A comparison with a brick-shaped, simplified model showed that conduction depended to a moderate extent on the shape of myocytes; a comparison with a one-dimensional bidomain model with the same overall shape and structure showed that the apparent conductivity of the tissue can be used to create an equivalent bidomain model. In summary, the microdomain approach offers a means of directly incorporating structural and functional parameters into models of cardiac activation and propagation and thus provides a valuable bridge between the cellular and tissue domains in the myocardium.

Keywords—Cardiac tissue, Computer model, Propagation, Simulation.

INTRODUCTION

Simulating the spread of electrical activity in cardiac tissue is a useful tool in understanding the mechanisms behind processes such as arrhythmias and defibrillation.[31] The advantage of computer simulations is that one can compute electrical potentials and currents with a resolution no experimental method can achieve. However, in order to be useful, the simulations need to produce realistic results that resemble experimentally observed values. In order to obtain enough accuracy to capture features like the genesis of arrhythmias, the simulations should incorporate all the aspects of impulse propagation that play a role in depolarization. In this study we developed a discrete model of a small aggregate of cardiac myocytes and used it to improve the accuracy of the bidomain model, a widely used and efficient approach for simulating whole heart electrophysiology.

In order to reduce numerical complexity, the bidomain approximation,[12,13,31] makes assumptions about the morphology of the tissue structure. The bidomain assumes that cardiac tissue contains both intracellular and extracellular domains that coexist at each location within the myocardium; the membrane connecting both spaces is similarly present at each location in space.[13] In this continuous representation, the electrical properties are characterized by two independent conductivity tensors: one for the intracellular space and one for the extracellular space. The bidomain formulation is completed by a membrane equation that describes the dynamics of the ionic currents flowing between both domains through ion channels and pumps located inside the membrane.

The bidomain approximation achieves its efficiency by not taking into account the microscopic mechanisms that control the spread of activation between myocytes, a trait that limits its utility in questions such as the role of changes in myocardial structure that arise during ischemia.[29] In order to fill the gap between the models that describe the electrical behavior for single cells and the continuous tissue models like the

Address correspondence to Jeroen Stinstra, Scientific Computing and Imaging Institute, University of Utah, 72S Central Campus Drive, 3750 WEB, Salt Lake City, UT 84112, USA. Electronic mail: jeroen@cvrti.utah.edu

bidomain, we created a model of cardiac tissue that includes a network of explicit cells and we used it to study the electrical phenomena that occur at this interim level. Such a model is not meant to replace the bidomain model, because it will not scale as efficiently. Rather the goal of the microdomain model was to employ a highly resolved model of a small number of cells to evaluate behavior and generate parameters that then feed into a bidomain.

We introduce here a model of cardiac tissue that extends the ideas of Spach *et al.*'s studies into three dimensions and includes a discrete localized extracellular space, thus addressing one of the limitations of their approach. Spach,[25] created a two dimensional model of cardiac tissue by extracting the outlines of myocytes from microscopic images and connected these pieces together into a lattice to form a cross section of cardiac tissue. They set the potential of the outside of each myocyte to ground, which assumes a highly conductive extracellular space overlaying the model. The myocytes in their model were coupled by discrete connections representing the intercalated disks containing different numbers of gap-junctions depending on the location of the connection. The major limitation of this approach is that in a two-dimensional model, the extracellular space and the intercellular space cannot be intertwined and at the same time form a continuous space, whereas in a three dimensional model all the myocytes can be connected through gap-junctions to form one continuous space, wrapped inside a fully connected extracellular space. In a two-dimensional model the only way to ensure that both intracellular and extracellular spaces are fully connected, is to make assumptions similar to the bidomain model in which two spaces coexist in the same space, but do not share the same potentials. By creating a discrete three-dimensional model with explicit extracellular space, we sought to evaluate the assumptions inherent in the bidomain formulation and to avoid complications associated with limitations of a two-dimensional model.

Creating a histologically realistic model of myocardium in three dimensions is substantially more challenging than in two because it requires extracting myocyte shapes from microscopy through segmentation of a stack of images. Hence, we followed a different approach from Spach[25] and developed an algorithm that rendered shapes of cardiac myocytes that were controlled by histological parameters, but were constrained to fit together like a jig-saw puzzle. We first developed this approach for predicting the passive bidomain conductivities of cardiac tissue based on histological parameters such as cell length and cross section.[27,29] That model did not include any active membrane currents, i.e. it was a fully passive model,

and was based on a small piece of myocardium (64 cells) with explicit extracellular and intracellular spaces. In this study, we expanded this modeling approach to include an active membrane that could be stimulated to initiate a propagating depolarization front. The scale of the model also grew to 1.5 mm (132 cells) in order to simulate realistic spread of activation.

As a final component, we created a more schematic version of the model with very regular cells of constant cross section and length in order to study the influence of the myocyte shape and layout on the propagation of action potentials. We then derived from both models the macroscopic parameters necessary to create an equivalent bidomain model and were able to compare the behavior of all three.

Without any adjustments of parameters to achieve specific results, we were able to replicate realistic planar propagation velocities in all three models. Thus we were able to show that it is possible to create models from very basic assumptions about parameters like the conductivity of electrolytes and distributions of gap junctions combined with realistic geometry of myocytes and extracellular space. The significance of these results lies in the leverage they now provide to include specific variations in cell and tissue parameters that are known to arise in pathology and translate these variations into estimates of the associated macroscopic parameters that can drive a (more efficient) bidomain solution of the whole heart.

METHODS

Overview

The aim of the model was to simulate a realistic spread of activation through a small piece of anisotropic myocardium at the highest tractable detail. Key components of the model were the shape of the individual myocytes, the coupling of myocytes through gap junctions, the current paths inside the intracellular or extracellular spaces, and the ion channel distribution. The three main components of the model were: (1) the geometrical model that described how these key components are organized in space, (2) the electrical model that described the electrical behavior for each of these components, and (3) the simulation software that combined the geometrical and electrical model into a physical model and simulated propagation in three dimensions.

Geometrical model

The geometrical model consisted of an explicit description of the shape and stacking of all the

myocytes that are located in the piece of tissue to be simulated. The intracellular and extracellular spaces were continuous and spatially separate volumes, but unlike the bidomain, these two volumes were defined inside the same Cartesian space.[29] Hence, in our model the myocytes did not fill the full space of the tissue, but left space for the extracellular matrix that surrounded the myocytes. We assumed that the myocytes were stacked inside an extracellular matrix so that at some locations, the myocytes touched neighboring myocytes, whereas at other locations small sheets of extracellular space separated the myocytes. Hence in this model the tissue was subdivided into multiple non-overlapping compartments: a single compartment for the extracellular space and separate compartments for each myocyte in the model.

A general goal of this study was to create an approach to model generation that would allow us to incorporate highly realistic features of myocardial structure and yet be able to implement variations in structure that represented both naturally occurring variation and systematic shifts that arise from pathology. Thus it was essential to develop an algorithm that was based on histological data and yet allowed variation based on control parameters to generate a range of specific models. To meet these requirements, we used an approach from a previous study to predict values for the impedances of cardiac tissue[27,29] that was based on seeding centers of cells and growing them together while constraining the shape to resemble myocytes captured in histology. One advantage of this approach is that it allows for control over histological parameters such as myocyte length and cross section. Another advantage is that such a model supports the generation of very tightly packed stacks of myocytes with extracellular space of less than 10% of the total volume, a very realistic value based on studies from the literature.[14]

Figure 1 illustrates our process of generating a geometrical model of cardiac tissue. The top panel in Fig. 1 depicts the regular grid that was used to grow the shapes of the myocytes. The first step in the process was the creation of cross-sections perpendicular to the fiber axis by growing individual myocytes from seed points. The process was accomplished by repetitively expanding the boundary of each myocyte by adding randomly chosen unassigned elements of the grid to each cross section until every element in the grid had been assigned to a myocyte.

These cross sections were then inserted into a three-dimensional grid, as depicted in Panel B. Each of the cross sections was now expanded into the third dimension by growing the elements along the fiber axis. The length of each resulting column was then chosen at random, while maintaining a spatial correlation with the lengths of neighboring rows. Only at the start and the end of the bundle was space left unassigned to form an extracellular bath on both ends of the fiber.

Panel C demonstrates the process of creating the extracellular space between the myocytes. To generate a smoother shape of the initial myocytes, each hexahedral element in the grid was replaced by six prisms, some of which had an additional layer of prisms on the outside to represent the extracellular space. This procedure resulted in a full separation of the myocytes by thin sheets of extracellular space, as shown the in output mesh in Panel C. Because each subsequent cross section had a different layout of myocytes, the sheets of extracellular space did not line up and myocytes were connected to each other through the surfaces perpendicular to the fiber direction. As a consequence, the myocytes were surrounded on four sides by extracellular space and on two sides by neighboring myocytes. The result was a jig-saw like stack of myocytes connected to each other by intercalated disks and at the same time were separated from each other by thin sheets of extracellular space that formed a continuous space. In a final step, all the elements were broken down into tetrahedra, creating a model like the one shown in Panel D. In this figure, each differently colored space represents a different myocyte and the extracellular space is transparent.

Electrical Model

In the classic bidomain theory, the electrical properties of the tissue are summarized by two conductivity tensors and an active membrane equation that describes the ionic current flow between both spaces. Because in our approach space is subdivided into a set of discrete rather than continuous spaces, the governing electrical equations had to be reformulated to fit the geometrical model. Additionally, in our formulation the intracellular and extracellular spaces were separated by surfaces that represented the shape of the actual cell membrane. In the model description we made a distinction between three types of separation surfaces (a surface that separated the different domains of the model): (1) surfaces that separated the intracellular from the extracellular space that were modeled by equations describing the ionic currents flowing through the membrane, (2) surfaces that separated two intracellular spaces and were assumed to be infused with intercalated disks that connected the two neighboring myocytes by means of gap junctions, and (3) surfaces that formed the outside boundary of the model. Each of the volumes in this formulation *was* bounded entirely by a combination of these three types of surfaces.
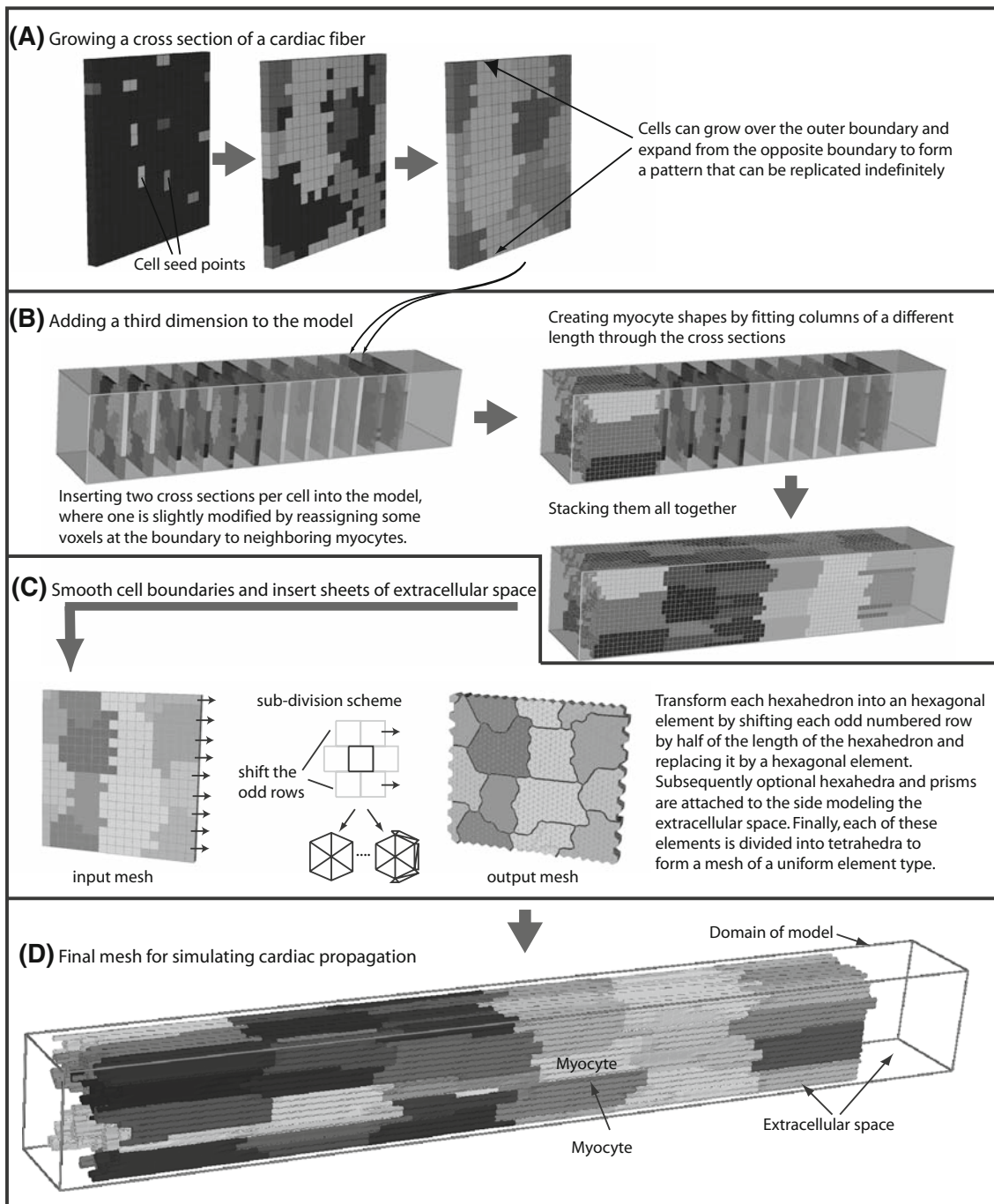
FIGURE 1. Creating a geometric model of cardiac tissue. Panel A depicts the growth of a cross section with myocyte shapes inside a regular grid from seed points. Each color represents a different myocyte. Panel B shows how these cross sections are inserted into a 3D stack and how a 3D model of the myocytes is created by filling the spaces between the cross sections. Panel C shows the steps that transform the regular mesh to more smoothly shaped myocytes that are separated by a small amount of extracellular space. This process is accomplished by augmenting hexahedral elements in the regular mesh with an optional thin sheet of extracellular space at the boundaries where two cells are connected. Panel D shows the final result of a small section of a cardiac tissue fiber with irregularly shaped myocytes inside an extracellular matrix. The box around the model shows the full extent of the model; the space that is left open is filled with extracellular space and the colored shapes represent individual myocytes in the cardiac muscle.

In order to simulate the propagation of action potentials, we assumed that each individual volume could be described as a homogeneous, isotropic, and linear volume conductor.[1,11] The characteristic conductivities of the intracellular and extracellular spaces were spatial homogenizations of the components

within each space. For example, for the intracellular space we assumed a conductivity that accounts for the organelles by averaging the conductive properties of the intracellular electrolyte over the full space of the myocyte. As the model simulated relatively slowly changing potentials (below 1 kHz), the dielectric and inductive properties of each of the volume conductors could be ignored.[18] Under these assumptions and the notion that the intracellular and extracellular spaces did not contain any electrical sources, the potentials inside each volume conductor could be obtained by solving a series of Laplace's equations with the proper boundary conditions:

$$\nabla \cdot \sigma_i \nabla \phi_i(\vec{r}) = 0 \qquad (1)$$

$$\nabla \cdot \sigma_e \nabla \phi_e(\vec{r}) = 0, \qquad (2)$$

where σ_i and σ_e are the conductivities of the intracellular space and extracellular space respectively, and $\phi_i(\vec{r})$ and $\phi_e(\vec{r})$ are the electrical potential in the intracellular and extracellular space respectively. Unlike the classical bidomain equation, we assumed that there were no sources inside each of the volumes and hence the right hand side term was equal to zero. Instead, in this formulation, all the source terms were integrated into the boundary conditions. Firstly, for the surfaces separating the intracellular and extracellular spaces we used the following set of boundary conditions:

$$
\begin{aligned}
(\sigma_i \nabla \phi_i(\vec{r})) \cdot \vec{n} &= -(\sigma_e \nabla \phi_e(\vec{r})) \cdot \vec{n} \\
&= I_{mem}(\phi_i(\vec{r}) - \phi_e(\vec{r}), q_1, \ldots, q_n) \\
&\quad + C_m \frac{\partial(\phi_i(\vec{r}) - \phi_e(\vec{r}))}{\partial t} + I_{stim}(t), \quad (3)
\end{aligned}
$$

where $\vec{n}$ denotes the normal vector at the boundary, C_m is the membrane capacitance per unit area, I_{stim} is an externally applied stimulus current, I_{mem} are the ionic currents per unit membrane surface, and q_1 to q_n are the variables denoting the state of the membrane as a function of time. We used the Luo-Rudy I ionic current model formulated to simulate the currents in a ventricular myocyte of a guinea pig,[15] which contains a good description of the upstroke of the action potential at a reasonable computational cost.

For boundaries separating two myocytes, we assumed a surface resistance and capacitance that mimicked a membrane infused with gap junctions, i.e. a low resistive barrier between the two myocytes. The following boundary conditions were applied to these surfaces:

$$(\sigma_{i1} \nabla \phi_{i1}) \cdot \vec{n} = C_m \frac{\partial(\phi_{i1} - \phi_{i2})}{\partial t} + G_{icd}(\phi_{i1} - \phi_{i2}) \quad (4)$$

$$(\sigma_{i2} \nabla \phi_{i2}) \cdot \vec{n} = -C_m \frac{\partial(\phi_{i1} - \phi_{i2})}{\partial t} - G_{icd}(\phi_{i1} - \phi_{i2}) \quad (5)$$

where G_{icd}, the conductance of the intercalated disk, is defined as

$$G_{icd} = \frac{1}{\rho_s} \qquad (6)$$

and where ρ_s is the effective surface resistance of the membrane due to gap junctions. We assumed that gap junctions were formed everywhere where two cells touch and that the connexons that form the gap junctions were homogeneously distributed over those parts of the membrane.
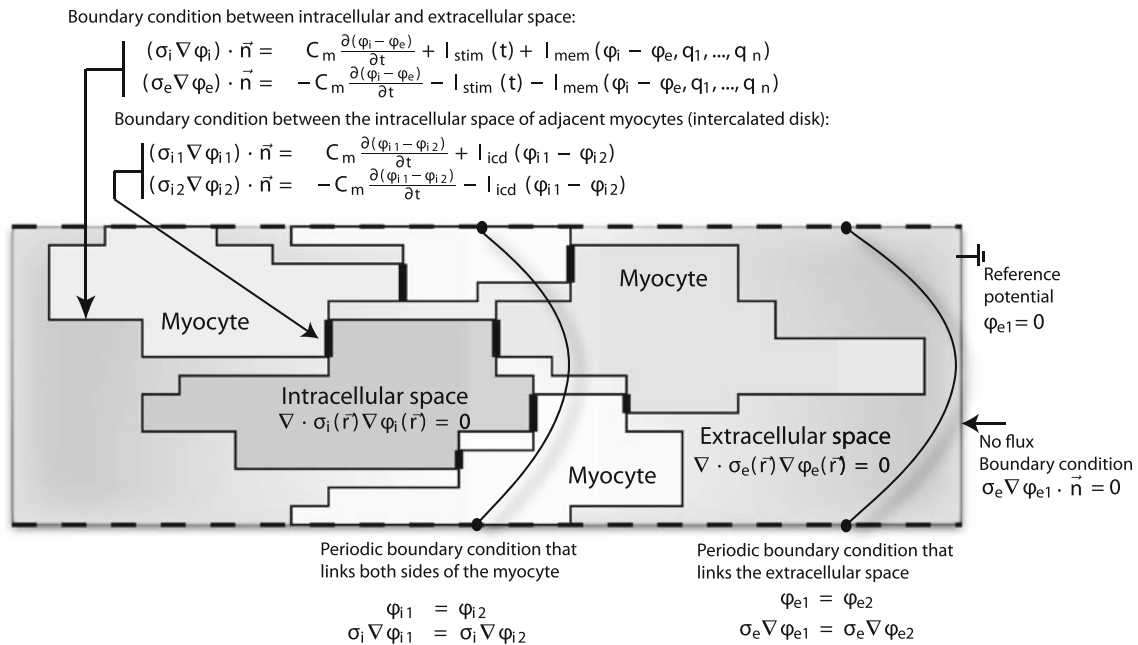
Finally, at the two outer boundaries at the end of the model we assumed a non-flux condition:

$$\sigma \nabla \phi_e \cdot \vec{n} = 0 \qquad (7)$$

At the other four side boundaries we assumed periodic boundary conditions, i.e. the potentials at opposite nodes of the finite element model were set to be equal and the current flowing out of the domain was forced to reenter the domain at the opposite boundary of the periodic domain.[27]

This assumption allowed us to replicate the model of the small piece of tissue indefinitely along the two axes perpendicular to the fiber direction, and thus create an infinite slab of tissue that was bounded only at the start and at the end of the fiber. As each of the replicated pieces was surrounded by the same tissue pieces, the potential distribution inside each of them was equal, at least when the same myocyte stacking applied to each of these replicated pieces. This concept has the advantage that one only need compute the potentials inside a small piece of tissue in order to obtain the full solution of a wavefront traveling through a thin slab of tissue. Figure 2 depicts a summary of all the model equations and boundary conditions. However, in the direction along the fibers we could not apply these periodic boundary conditions, as the planar depolarization wave was traveling in this direction, resulting in polarized membranes on one side and depolarized membranes on the other side. In other to reduce the amount of border effects, we modeled as many myocytes in this direction as our simulation software could handle.

The choices of the electrical passive parameters for the model were based on previously published values.[27] The conductivity of the extracellular space was 20 mS/cm, which is similar to the conductivity of other bodily fluids with the same concentrations of sodium and chloride (the two ions mainly responsible for conduction).[2,30] Conductivity in the intracellular space was 3 mS/cm, a value derived from experiments by Brown *et al.*[3] Gap junctions had an effective surface

Boundary condition between intracellular and extracellular space:

$$(\sigma_i \nabla \varphi_i) \cdot \vec{n} = \quad C_m \frac{\partial(\varphi_i - \varphi_e)}{\partial t} + I_{stim}(t) + I_{mem}(\varphi_i - \varphi_e, q_1, ..., q_n)$$

$$(\sigma_e \nabla \varphi_e) \cdot \vec{n} = \quad -C_m \frac{\partial(\varphi_i - \varphi_e)}{\partial t} - I_{stim}(t) - I_{mem}(\varphi_i - \varphi_e, q_1, ..., q_n)$$

Boundary condition between the intracellular space of adjacent myocytes (intercalated disk):

$$(\sigma_{i1} \nabla \varphi_{i1}) \cdot \vec{n} = \quad C_m \frac{\partial(\varphi_{i1} - \varphi_{i2})}{\partial t} + I_{icd}(\varphi_{i1} - \varphi_{i2})$$

$$(\sigma_{i2} \nabla \varphi_{i2}) \cdot \vec{n} = \quad -C_m \frac{\partial(\varphi_{i1} - \varphi_{i2})}{\partial t} - I_{icd}(\varphi_{i1} - \varphi_{i2})$$

Myocyte

Myocyte

Reference potential
$\varphi_{e1} = 0$

Intracellular space
$\nabla \cdot \sigma_i(\vec{r}) \nabla \varphi_i(\vec{r}) = 0$

Extracellular space
$\nabla \cdot \sigma_e(\vec{r}) \nabla \varphi_e(\vec{r}) = 0$

Myocyte

No flux
Boundary condition
$\sigma_e \nabla \varphi_{e1} \cdot \vec{n} = 0$

Periodic boundary condition that links both sides of the myocyte

$$\varphi_{i1} = \varphi_{i2}$$
$$\sigma_i \nabla \varphi_{i1} = \sigma_i \nabla \varphi_{i2}$$

Periodic boundary condition that links the extracellular space

$$\varphi_{e1} = \varphi_{e2}$$
$$\sigma_e \nabla \varphi_{e1} = \sigma_e \nabla \varphi_{e2}$$

FIGURE 2. A schematic overview of the physical model. This figure depicts the partial differential equations that describe the potential in each domain and their boundary conditions. Depending on whether the boundary is between the extra- and intracellular space or between the intracellular spaces of two myocytes, a different boundary condition is applied. The figure also depicts the boundary conditions at the outer boundary, where the two ends of the model allow no current flux (solid line) and the other four sides mirror the potentials and currents on opposite sides of the model (dashed line).

resistance of 0.0015 kΩ cm^2, a value close to what we used in earlier studies and consistent with literature.[16,27] Finally we assumed a typical membrane capacitance of 1 μF/cm^2.[22] Although we kept them constant for this study, the methodology presented allows for spatially or temporally changing these parameters.

Computation Model

The discretization of the spatial model was based on a mesh that consisted of tetrahedral elements obtained by dividing the elements of the geometrical model (a combination of hexahedra, prisms, pyramids and tetrahedra) into tetrahedra. All boundaries between the different domains coincided with interfaces between the elements. Since the potential distribution is discontinuous over the internal boundaries of such a model, i.e. there is a potential difference over each membrane, the mesh was split at the nodes that were located at these boundaries, resulting in a number of unconnected meshes, one for each domain. As the internal membranes in the model were assumed to be infinitely thin, corresponding nodes from either side of the internal boundary were located at the same Cartesian coordinates. This resulted in interpolated potentials between nodes of the same domain and a finite potential difference over each internal boundary. The final model consisted of elements whose nodes

were separated by distances ranging from 0.2 μm in the extracellular space to 5 μm in certain areas of the intracellular space.

To solve for the potential, we used the finite element method with linear interpolation inside each element. This allowed us to generate a stiffness matrix for each part of the model using a Galerkin based finite element approximation. For the potentials and current densities at the boundaries, we assumed a linear interpolation over each triangular face of the outer boundary of each domain. To evaluate the amount of current flowing through each membrane element, the current density was computed for each corner node using potential difference over the membrane at that node. That current was subsequently linearly interpolated on the surface and was used as a source term to solve the finite element model of each domain. Because a myocyte is surrounded by extracellular space and neighboring myocytes, some surface elements were designated as intercalated disks, whereas other were designated as plasma membrane, both with different equations governing the membrane current.

To solve for the potential in space and time, we used a semi-implicit Crank–Nicolson scheme[7] and solved the linear set of equations that resulted from the finite element method for each time instant using the Minimal Residual Method (MINRES). As an initial guess for each solve, we used a linear prediction based on the

two previous time steps. For the time steps we used a time adaptive version of the semi-implicit Crank–Nicolson scheme[28] based on the maximum derivative of the membrane potential.[15] The resulting adaptive time stepper ranged between 50 ns and 5 μs. The state of the membrane was initialized by a stimulation series at 2 Hz first applied to a simpler model.[29]

The mesh and the finite element models were implemented with the SCIRun software package (http://software.sci.utah.edu), and a solver first implemented in the CardioWave (http://cardiowave.duke.edu) framework[28] that was designed to solve multiple finite element models with parallel implementations of membrane models.

The simulation of propagation as depicted in Figs. 5 and 6 took about 36 h to evaluate on an Apple computer with two quad-core 3.0 GHz Xeon processors. Although not depicted here, we simulated one beat at different tolerances for the solver and at different mesh densities to confirm convergence of our solutions. In the results presented, we used a relative error of 3×10^{-6} for the iterative solution.

Schematic vs. Realistically Shaped Myocytes

To evaluate the role of myocyte shape on the spread of activation, for generating new insights into

mechanisms of cardiac conduction, we generated two models for this study, one based on schematic myocytes in the form of bricks and one that used realistically shaped myocytes based on histology. Figure 3 shows both models in cross sections along and across the cardiac fiber. Both models consisted of 132 myocytes, and had the same outer dimensions. Each model had approximately 540,000 nodes and about 93,000 were membrane nodes each of which required the solution of a full set of membrane equations.

RESULTS

Qualitative Comparison with Histology

Figure 4 depicts a qualitative comparison between shape and stacking of the myocytes as generated by our algorithm and histology. The upper panel depicts typical shapes of individual myocytes in the computer model (left) and actual confocal images of ventricular myocytes (right). The shape of each myocytes can be characterized as a set of small bundles consisting mainly of actin/myosin fibers and mitochondria[10,24] that are stacked on top each other, but have different lengths. Although the shape of a myocyte approximates a brick with the length along the fiber direction
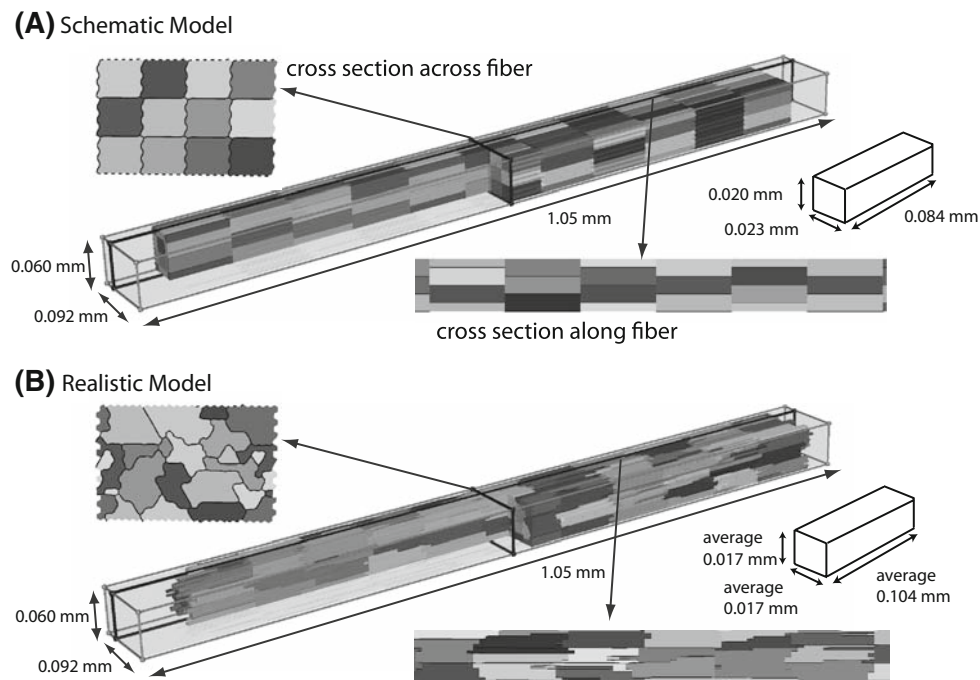

FIGURE 3. A comparison between the two types of models that were generated for this study. Panel A shows a schematic model that was created by using a square cross section, which was stacked with no irregularities along the z-axis. Panel B shows a similar model but with a more realistic cross section and an irregular stacking along the z-axis. Both panels show the 3D layout of model as well as cross sections perpendicular and parallel to the fiber orientation. To the right the approximate dimensions of each cell is depicted. Note that for the irregular stacking the dimensions are average dimensions as each cell has a different dimension.

(A) Cell shape

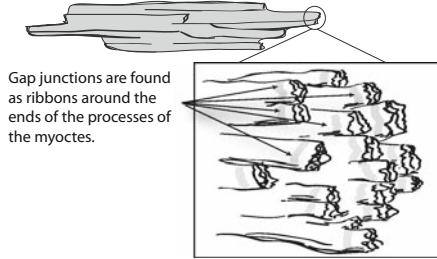Cell shapes in the computer generated model :

Microscopic images of rat myocytes for comparison:
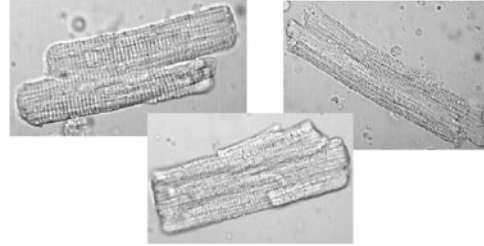
(B) Gap junction distribution

Location of gap junctions as discussed by Hoyt et al. [14] :
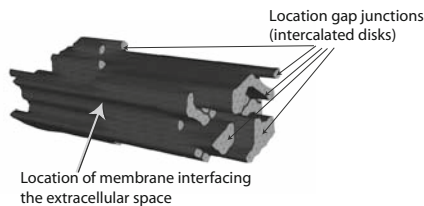
Distribution of gap junctions in our model:

Cross section through the model: showing intracellular space (light brown); extracellular space (dark brown), and gap junctions (white)

Gap junctions are found as ribbons around the ends of the processes of the myoctes.

Extracellular space   Small lateral connections

Myocyte   Myocyte   Myocyte
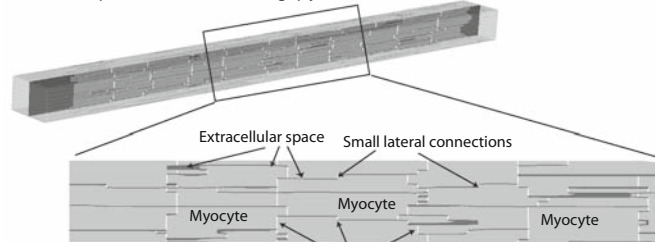
Gap junctions

Location of gap junctions assumed in our model :

Location gap junctions (intercalated disks)

Cross section of bundle showing distribution of gap junctions in one plane along the bundle (visualized as if it were a histological labeling of connexin 43) :
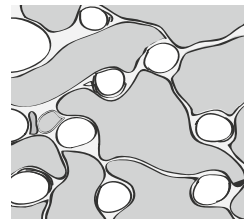
Location of membrane interfacing the extracellular space

(C) Extracellular space

Distribution of extracellular space around myocytes :
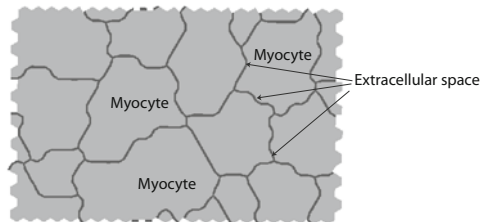
Sketch of cross section of cardiac tissue based up on histology images by Forbes and Sperelakis [8] :

Myocyte

Extracellular space

Myocyte

Myocyte

FIGURE 4. **A comparison between the computer generated tissue geometry and actual samples/illustrations from histology. Panel A depicts a comparison of the shape of the cells. On the left side of the panel are examples of the computer generated myocytes and on the right side, confocal microscopy images of actual myocytes. Both images display the general brick like shape of the myocytes with stair step irregularities at the ends and sides of the myocytes. Panel B depicts an illustration of the locations of the gap junctions (gray bands at the end of the processes) as discussed by Hoyt *et al.*[14] in the upper left corner. In the lower left corner of the same panel, the brightly colored surfaces depict the locations of the gap junctions. On the right side of Panel B, the distribution of the gap junctions in the model is demonstrated. The figure in the middle renders a close up of locations of gap junctions in relation to the extracellular space and the lower figure highlights the distribution of the gap junctions in a slice along the fiber with all the other model details hidden. Finally, Panel C depicts the extracellular space that surrounds the myocytes in the model on the left and a drawing of the extracellular space based on images of histology such as those given by Forbes and Sperelakis.[8]**

of the muscle being about 5 times as large as the two other sides, a close inspection shows that the ends form a stair step cross section.[8,24] Although the comparison in Panel A is only qualitative, it shows that the computer generated model captures both the overall brick

like shape as well as the stair stepped details of the ends of the myocytes.

A further simplification of the model was necessary to accommodate the effects of the locations of gap junctions in real myocytes. The figure in the upper left

corner of Panel B illustrates the locations of the gap junctions as described histologically by Hoyt et al.[14] They found that the majority of gap junctions are located in small bands that circumvent the ends of the processes. These processes of the myocytes end in a very irregularly shaped surface in which most of the lateral overlap between the myocytes is infused with gap junctions. As this level of detail was too high for the model, we assumed that these interfaces were flat and perpendicular to the cardiac fiber. Thus the locations of the gap junctions were not on the lateral ends of the myocytes, but rather embedded throughout all the surfaces at the ends of the small processes. The latter is depicted in the lower left figure of Panel B. The combination of the choice of this location for the gap junctions with the irregular shapes of the myocytes generates the distribution of gap junctions within the tissue model, illustrated in the right hand side of Panel B.

We also compared the distribution of gap junctions in a cross section (Fig. 4, Panel B) with the histological results by Peters et al.,[17] who showed the distribution of gap junctions for various ages of human myocardium. The format of these visualizations is meant to compare with confocal microscopy studies with antibodies which typically capture only one plane and mainly highlight the location of the gap junctions. Our distribution compared well to that of Peters et al.[17] for mature cardiac tissue, in which most gap junctions were located at the ends of the myocytes on the surface perpendicular to the fiber direction and only a few were connecting the myocytes laterally.

Finally, Panel C in Fig. 4 depicts the distribution of extracellular space. As the amount of extracellular space was distributed in very thin sheets around the myocytes, we could compare our distribution with electron microscopy images of cardiac tissue. Panel C contains a cross section of the model along with a figure from Forbes and Sperelakis.[8] Although the thickness of the thin sheets of extracellular space in the model and actual tissue were similar, real tissue displays more variation in the thickness than the model. Similarly, in order to restrict the complexity of the model, we did not include capillaries, which are known to occupy a certain amount of volume. As a result we chose a smaller volume fraction for the extracellular space, which normally includes capillaries. However the conductive properties of the capillary walls are low and currents flowing along the capillaries are largely restricted by red blood cells.[27] Hence most of the capillary system will be electrically isolated from the interstitial space surrounding the myocytes directly. Hence in this study we opted for the approximation of assuming that no currents will flow through the capillary system.

Quantitative Comparison with Histology

Past investigators have reported a number of characteristic values to describe myocardial tissue and we adjusted parameters of the computer algorithm to match these metrics. These parameters of the model included the dimensions of the hexahedral grid, the blurring parameters in generating the cross sections, and the average distance between cross sections. As these parameters did not map directly to metrics reported in literature, we varied them over a wide range in order to match previously reported values. The resulting average myocyte length in the model was 104 μm and the average cross section (cell volume divided by cell length) was 284 μm^2, which is in the range reported by Campbell et al.[4] for several mammalian species, with a myocyte length between 83 and 130 μm for the left ventricle and cross sections ranging from 139 to 364 μm^2. In our geometric model, each myocyte was connected to 11 other myocytes, which was in the range reported by Hoyt et al.[14] of 9 $\pm$ 2. In our model 7% of the cell membrane was composed of the gap-junctions; Hoyt et al.[14] reported a percentage of 5.2% of the membrane that was infused with gap-junctions. The intracellular volume fraction for the bundle was 93%, which is close to the value reported by Hoyt et al. of 92%.

Simulation of Conduction Velocities in a Bundle of Cardiac Tissue

To evaluate the functional characteristics of the model, we carried out simulations of the spread of activation along the fiber direction by stimulating the membranes of the first layer of myocytes as depicted in Fig. 5 and monitoring the resulting propagated excitation. The stimulated portion of the membrane is depicted in red, whereas the other segments of the membranes are rendered transparently with the locations of the gap junctions as solid blue surfaces. The middle three panels of Fig. 5 show the transmembrane, extracellular, and intracellular potentials as functions of space for a time instant at which the depolarization wave was about half way down the fiber. The figures show that all three potentials changed gradually from a polarized state to the depolarized state over a length of about 3 myocytes. In the lower panel are five time signals from equally spaced locations along the fiber that show the typical upstroke in transmembrane potential with edge effects accounting for the altered morphology of the first and last signal. The intracellular and extracellular potentials also showed rapid, substantial changes of opposite polarity, showing that the transmembrane potential was as much a function of a initially
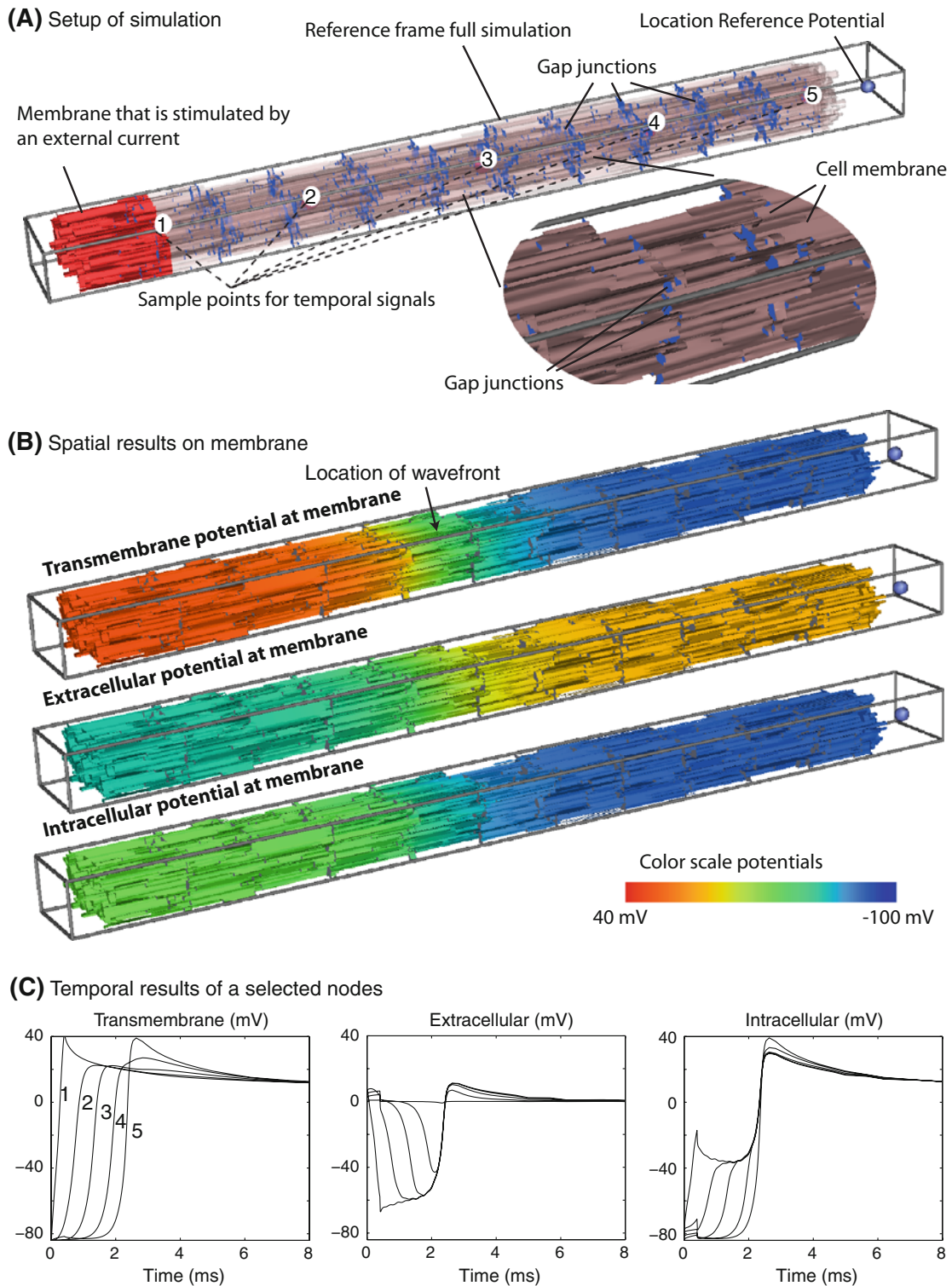
FIGURE 5. The setup of the propagation simulations. Panel A shows the layout of the model with membranes shown transparently in brown and the intercalated disks shown in blue. This bundle is stimulated on the left by adding an impressed current on the membranes colored in red. Panel B shows the potential at one point in time where the depolarization front is about half way down the bundle. In this panel, the transmembrane, the extracellular, and the intracellular potentials are displayed using color scales. Panel C depicts the shapes of these three potentials in time for five nodes along the fiber.

increasing intracellular potential as it was of the initially decreasing extracellular potential.

In order to compute the activation times of the membrane and estimate conduction velocities, we defined the time of activation in the conventional manner as the time instant of the steepest upstroke of the action potential. By computing the average activation times within two cross sections of the bundle as depicted by Fig. 6, we computed the conduction velocities by measuring the distance the wave traveled between the two cross sections. Figure 6 contains an example of such an activation map, in which blue indicates early activation and red late activation.

The value of dV_m/dt is also a sensitive metric of the spread of activation and here, too, our results agreed well with experiments. The lower image of Fig. 6 depicts the maximum upstroke at the time of activation, showing anomalous upstroke values in the first three cell layers as well as in the last due to the stimulus current and boundary effects at the end of the fiber. This result is consistent with those of Spach et al.[26] who showed that the upstroke depends on boundary effects and loading of the membranes. In order to avoid bias in the computation of the conduction velocity, we only used the center of the bundle, where parameters such as the upstroke are relatively homogeneous.

One question we addressed that is of great practical consequences is whether the additional complexity of the realistic call model actually resulted in more accurate results. To test this hypothesis, we compared the conduction velocity for a fiber bundle constructed from both brick-shaped myocytes with one based on more realistic shape for three different thicknesses of the sheet of extracellular space. The results are summarized in Table 1 and show very similar conduction velocities. The table also shows the effective conductivities of the volume for both the intracellular and extracellular space, which shows that the geometry also has an effect on the effective conductivity and that the values we obtained are comparable with the numbers we estimated in an earlier study.[27] Although the thickness of the layer of extracellular space was the same for both model types, the overall amount of extracellular volume differed slightly; as the realistic shape of the myocytes meant that they had a larger surface area and hence more extracellular space. Only for the largest extracellular space layer the computed conduction velocities of 0.43 and 0.45 m/s for the realistic and schematic models, respectively, were close to the value of 0.48 ± 0.04 m/s reported by Clerc.[6]

Influence of Myocyte Shape

One of properties of the classical bidomain models is that the transmembrane potential shows a smooth profile from the depolarized zone into the repolarized zone. In order to evaluate this aspect of the effect of a discrete model, we plotted the transmembrane potential as a function of the distance along the fiber (Fig. 7). The figure shows that the profile of the transmembrane potential generally follows a smooth transition along the fiber.
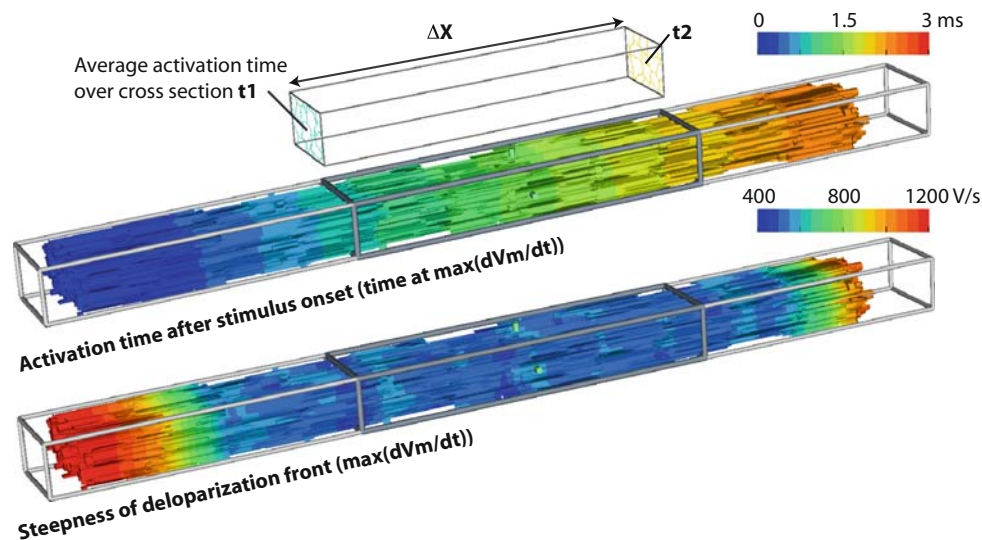
FIGURE 6. Calculation of propagation velocities. The figure depicts the activation time as a function of the location in the bundle. The propagation velocities were computed by taking two slices perpendicular to the fiber orientation at a separation of about 4 cells. For each slice, the average activation time was computed and the time difference along the fiber used to compute propagation speeds. The lower image shows the maximum value of dV_m/dt of the transmembrane potential, which was used to compute the activation times.

TABLE 1.   Conduction velocities for realistic and schematic models at different ratios of the extracellular space.

ECS thickness (μm)	Schematic model			Realistically shaped model		
	ECS (vol.%)	Velocity (m/s)	Effective [ICS/ECS] conductivity (S/cm)	ECS (vol.%)	Velocity (m/s)	Effective [ICS/ECS] conductivity (S/cm)
1.1	9.4	0.44	1.71/1.80	12	0.43	1.58/2.13
0.67	5.6	0.39	1.82/1.08	7.3	0.37	1.72/1.29
0.22	1.9	0.26	1.93/0.36	2.2	0.26	1.87/0.43
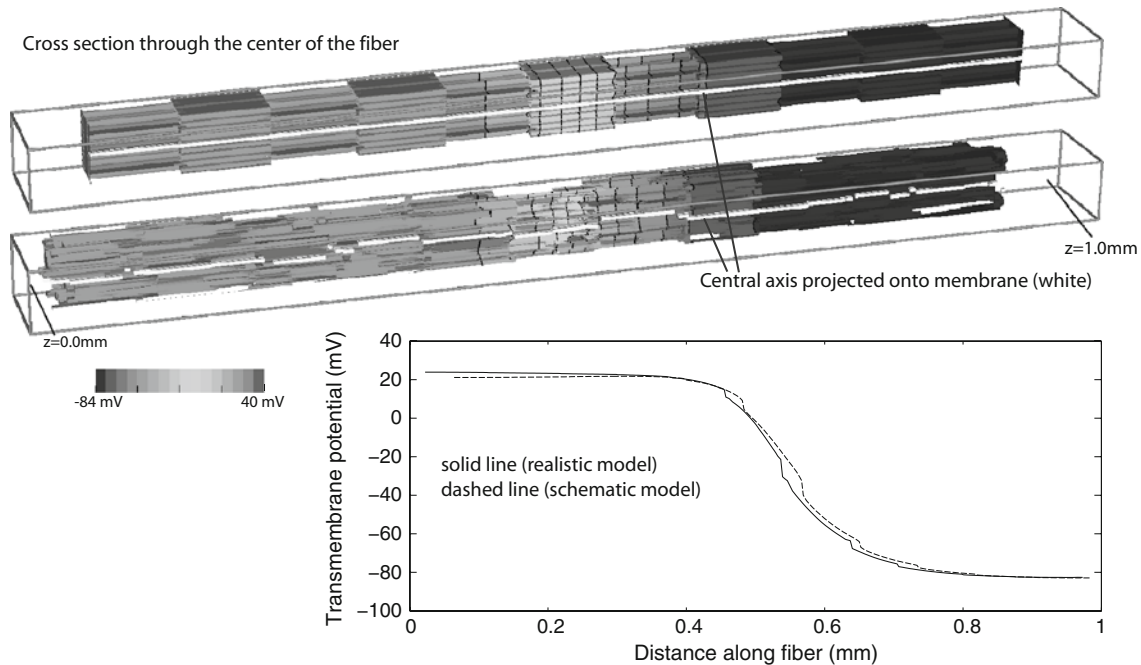
FIGURE 7.   Comparison between two models with differently shaped myocytes. The upper figure shows the comparison of the transmembrane potentials as a function of space for two models, one with brick shaped myocytes (schematic model) and one with irregular shaped myocytes (realistic model). The lower figure shows the profile of the transmembrane potential along the fiber. These values represent transmembrane potential on the closest membrane to the center line through the model. The white line in the two top figures shows the actual location that is followed for the lower figure.

Application of the Model

One natural application of a discrete microdomain model of cardiac cells is to compute equivalent parameters of simpler and more computationally efficient formulations such as the bidomain. To evaluate the accuracy of these parameters, it is then possible to apply them to a model formulated according to the bidomain approach and compare the resulting propagation characteristics between bidomain and microdomain models. We have used this approach previously for the computation of the passive electrical properties of the bidomain such as the effective intracellular and extracellular conductivity tensors[27] and extended the strategy here to propagation behavior. Figure 8 shows the scheme for carrying out such a comparison using a one-dimensional bidomain model and Table 2 summarizes the derived parameters and the resulting values for conduction velocity, for both realistic and schematic microdomain models.

DISCUSSION

The modeling approach presented in this study distinguishes itself from more traditional approaches by incorporating a detailed histological description of myocardial structure into a conduction model. The inclusion of these histological details voids the need for having to guess apparent tissue properties and results show that, in fact, realistic conduction velocities can be obtained based on the structural information, the electrical conductances of the electrolytes, and the membrane dynamics.
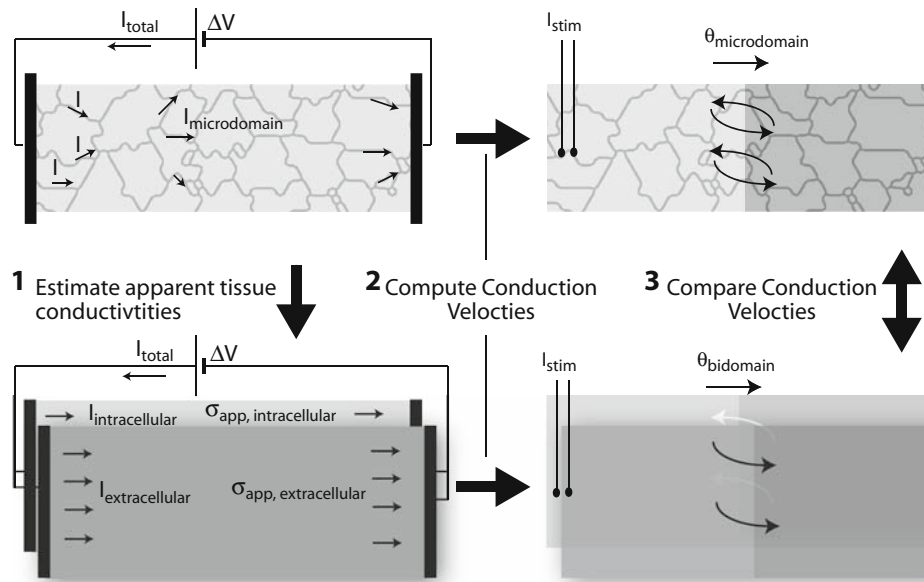
FIGURE 8. The scheme used to evaluate the relationship between the microdomain and bidomain models. By applying a homogeneous voltage gradient across a piece of tissue (upper left figure), it is possible to determine the resulting intracellular and extracellular currents within the model. One can then estimate the apparent conductivities of a bidomain model that results in the same currents within the tissue (lower left figure). These two modeling approaches can now be compared by simulating a propagating wave in both domains, (figures on the right) and determining conduction velocities (θ) for both cases.

TABLE 2. Comparison of microdomain and bidomain models.

	Realistic	Schematic
Conductivity ICS (S/m)	0.16	0.17
Conductivity ECS (S/m)	0.21	0.18
Surface–volume-ratio (1/m)	2.3×10^6	1.9×10^6
Conduction velocity bidomain (m/s)	0.415	0.449
Conduction velocity microdomain (m/s)	0.420	0.440

The table shows bulk tissue characteristics derived from both realistic and schematic microdomain models (upper three rows) and the resulting conduction velocities for the associated one-dimensional bidomain model and microdomain models.

This form of simulation model, which we describe as "microdomain", is meant to be a bridge between the discrete, explicit models of individual myocardial cells and the homogenized bidomain models, whose efficiency continues to enable steady progress in tissue and whole heart simulation. A microdomain model incorporates details of cell structure and organization and works at a spatial scale at which one can also include variations that arise under realistic physiological and pathophysiological conditions. This direct transfer of information at the histological scale into a simulation model is not possible with meso-scale approaches like the bidomain because it must be embedded in a small number of global parameters, i.e. the intracellular and extracellular conductivities. Hence our goal was to show that the microdomain models provide a direct

means to include histology and then generate simulation results on a small space scale that, in turn, can both validate and provide parameters for a bidomain model. Microdomain models also provide a means to convert or translate changes of shape, structure, or cellular composition from the cellular domain into bidomain parameter changes so that it becomes possible to improve the simulation of disease conditions in the bidomain.

Such a microdomain model is, of course, only as good as the histological information that drives it. In the case of myocardium, there is ample literature on some parameters such as cell size and distribution of gap junctions. In more qualitative parameters, such as myocyte shape, we have carried out visual comparison with the literature.[8,14,17] The presence of disease, especially with acute onset or rapid dynamics, is rarely captured in histology and for such scenarios, a microdomain model requires additional estimation. Thus, for example, one must estimate the extent and distribution of changes in extracellular space fraction that are known, at least in a qualitative sense, to arise during acute ischemia.[29] The advantage of the micro-domain approach we have implemented is that such changes are relatively simple to implement, as are other variations in fundamental values such as the conductivity of intracellular or extracellular ionic solutions.

A key step in proving the utility of the microdomain approach is validation of the results against valued from experiments. We have reported here results of

such validation based on the macroscopic parameter of conduction velocity. The realistically shaped myocyte model produced a conduction velocity of 0.43 m/s, which is only slightly lower than (and well within the error bounds of) the experimentally measured value of 0.46 ± 0.03 m/s reported by Cascio *et al.*[5] for papillary muscles. Cascio *et al.* also reported the voltage difference between depolarized and polarized tissue in the extracellular space and relate this to the ratio of the apparent intracellular conductivity vs. the apparent extracellular conductivity. The ratio they measured is close to one, similar to ratio we derived from histological measurements, indicating that the resistance the depolarization wave encounters is almost equally divided between the intracellular and extracellular space. However in our model the extracellular conductivity is a bit larger than the intracellular conductivity, while Cascio's measurements put the intracellular conductivity as the larger one. As shown in Table 1 when the extracellular space is reduced we obtain a similar ratio where the intracellular conductivity is larger than the extracellular one. In our model we assumed an extracellular space thickness of 1.1 μm and a volume fraction of 12%, which is in the range of experimental values for healthy tissue,[10] however those values were derived for the ventricular myocardium and not a papillary muscle. Hence to fully match the conductivity ratios reported by Cascio *et al.* the amount of space that contributes to the extracellular conduction may be slightly overestimated in this case.

Although the ratio of the apparent conductivities and the conduction velocity closely match the experimental results as reported by Cascio *et al.*,[5] the reported bulk conductivity of the papillary muscle of around 0.7 S/m (the sum of the apparent intracellular and extracellular conductivity) is larger than the value we derived of 0.37 S/m. However the value we derived is close to the experimentally reported value of around 0.4 S/m by Gabriel *et al.*[9] Moreover the value we derived is the apparent conductivity of the bundle of myocytes alone, whereas experimental values often include additional structures such as vascularity and layers of perfusate in the experimental setup, which may explain why reported literature values of the absolute tissue conductivity vary over a wide range. As our model predicts realistic conduction velocities and estimates the conductivities from independently obtained parameters, it provides additional help in scrutinizing literature conductivity values.

A critical feature of these results is that we optimized the geometrical model to fit the histological parameters reported in literature, rather than to fit a desired result (in the form, for example, of an expected propagation speed). The estimates of electrical parameters were based on physical properties like ion concentrations and ion mobilities; they were not adjusted to achieve a desired result. Hence, the predicted conduction velocities were based on parameters that were independently determined either from measurements or from first principles. Although these results do not exclude the possibility that other parameters not included in the model play an important role in cardiac conduction, it at least shows that a model with this level of detail is capable of generating realistic results. We have shown similar concordance in a previous study using the same geometric model to predict passive tissue conductivity tensors.[27,29]

Although histologically detailed models of cardiac tissue have been described, for example, the two-dimensional model developed by Spach,[25] this is the first three-dimensional model with realistically shaped myocytes that is large enough to simulate a realistic propagating wavefront. To compute simulations presented here with approximately 150 myocytes required about 48 h on a state-of-the-art multiprocessor computer. To achieve realistic propagation in a model of this size, we made special assumptions on the symmetry in order to warp the small cluster of 150 myocytes into a thin sheet of cardiac tissue, by replicating it indefinitely along two dimensions. Although this approach is valid to study phenomena such as the conduction of a planar wave, to simulate behavior such as reentry would require many more myocytes. Our approach is completely capable of such extensions, but for even moderately sized tissue volumes would require computational resources that outstrip current limits.

A feature of the model that provides additional flexibility is the ease with which parameter changes can yield new geometries that replicate abnormal physiological settings. For example, we have altered extracellular volume and ion concentrations to simulate acute ischemia and simulated their effect on conduction.[23] Moreover, we could alter parameters independently to evaluate their individual impact.

Another way in which we were able to adjust model parameters was to create a more schematic geometry and compare the resulting conduction velocity. Results of these simulations suggested that conduction velocity does vary with the shape of the myocytes, however the differences between the models were small in comparison to the range of experimental conduction velocities found in literature (0.4–0.7 m/s).[5,6,19,20] Another difference between the models was that along the fiber, the isochrones of activation were more regularly spaced in the realistically shaped model than in the schematic model, in which the depolarization front sped up toward the end of each cell and then slowed down at the start of the next cell. Similarly, the profile of the transmembrane potential as a function of the

distance through the fiber was smoother for the more realistically shaped model. Such results indicate that the realistic model better approaches the behavior of the homogenized bidomain as it displays a more constant conduction speed and a smoother transition of potential along the fiber, while the brick shaped model has the potential to overexpress the effects of discretization.

The modeling framework and associated software that we have developed is very flexible and supports the inclusion of additional compartments. For example, in a separate study, the same framework was adapted to replicate more asymmetric distributions in the extracellular space and showed associated changes in conduction velocities.[21] It would, for example, by straightforward to include the capillaries in such a model as long as their conductive characteristics were known.

In conclusion, we have demonstrated that a detailed model of cardiac tissue that results in realistic conduction can be constructed using only parameters from histology. This model generated values for propagation velocity that agree well with experiments without the need for adjustments in order to achieve such agreements. Each parameter of the model was justified entirely from independent histological studies. In addition, we have shown that even for relatively simple propagating plane waves, under simplifying assumptions of highly schematic organization of identical myocytes, the shape of the individual myocytes has some effect on propagation.

REFERENCES

[1]Barnard, A. C. L., I. M. Duck, and M. S. Lynn. The application of electromagnetic theory to electrocardiology. I. Derivation of the integral equations. *Biophys. J.* 7:433–462, 1967.

[2]Baumann, S. B., D. R. Wozny, S. K. Kelly, and F. M. Meno. The electrical conductivity of human cerebrospinal fluid at body temperature. *IEEE Trans. Biomed. Eng.* 44:220–223, 1997.

[3]Brown, A. M., K. S. Lee, and T. Powell. Voltage clamp and internal perfusion of single rat heart muscle cells. *J. Physiol.* 318:455–477, 1981.

[4]Campbell, S. E., A. M. Gerdes, and T. D. Smith. Comparison of regional differences in cardiac myocytes dimensions in rats, hamsters and guinea pigs. *Anat. Rec.* 219:53–59, 1987.

[5]Cascio, W. E., H. Yang, T. A. Johnson, B. J. Muller-Borer, and J. J. Lemasters. Electrical properties and conduction in perfused papillary muscle. *Circ. Res.* 89:807–814, 2001.

[6]Clerc, L. Directional differences of impulse spread in trabecular muscle from mammalian heart. *J. Physiol.* 255:335–346, 1976.

[7]Crank, J., and O. Nicolson. A practical method for numerical evaluation of solutions of partial differential equations of the heat-conduction type. *Proc. Camb. Phil. Soc.* 43:50–67, 1947.

[8]Forbes, M. S., and N. Sperelakis. Chapter 1—ultrastructure of mammalian cardiac muscle. In: Physiology and Pathophysiology of the Heart (3rd ed.). Norwell, MA: Kluwer Academic Publishers, 1995, pp. 1–35.

[9]Gabriel, S., R. W. Lau, and C. Gabriel. The dielectric properties of biological tissues: I. Literature survey. *Phys. Med. Biol.* 41:2231–2249, 1996.

[10]Gerdes, A. M., and F. H. Kasten. Morphometric study of endomyocardium and epimyocardium of the left ventricle in adult dogs. *Am. J. Anat.* 159(4):389–394, 1980.

[11]Geselowitz, D. B. On the magnetic field generated outside an inhomogeneous volume conductor by internal current sources. *IEEE Trans. Magn.* MAG-6(2):346–347, 1970.

[12]Harrild, D. M., and C. S. Henriquez. A computer model of normal conduction in the human atria. *Circ. Res.* 87:e25, 2000.

[13]Henriquez, C. S. Simulating the electrical behavior of cardiac tissue using the bidomain model. *Crit. Rev. Biomed. Eng.* 21:1–77, 1993.

[14]Hoyt, R. H., M. L. Cohen, and J. E. Saffitz. Distribution and three-dimensional structure of intercellular junctions in canine myocardium. *Circ. Res.* 64(3):563–574, 1989.

[15]Luo, C. H., and Y. Rudy. A model of the ventricular cardiac action potential. Depolarization, repolarization, and their interaction. *Circ. Res.* 68(6):1501–1526, 1991.

[16]Metzger, P., and R. Weingart. Electric current flow in cell pairs isolated from adult rat hearts. *J. Physiol.* 366:177–195, 1985.

[17]Peters, N. S., N. J. Severs, S. M. Rothery, C. Lincoln, M. H. Yacoub, and C. R. Green. Spatiotempoaral relation between gap junctions and fascia adherens junctions during human ventricular myocardium. *Circulation* 90:713–725, 1994.

[18]Plonsey, R., and D. B. Heppner. Considerations of quasi-stationarity in electrophysiological systems. *Bull. Math. Biophys.* 29:657–664, 1967.

[19]Roberts, D. E., L. T. Hersch, and A. M. Scher. Influence of cardiac fiber orientation on wavefront voltage, conduction velocity and tissue resistivity. *Circ. Res.* 44:701–712, 1979.

[20]Roberts, D. E., and A. M. Scher. Effect of tissue anisotropy on extracellualar potential fields in canine myocardium in situ. *Circ. Res.* 50:342–351, 1982.

[21]Roberts, S. F., J. G. Stinstra, and C.S. Henriquez. Discrete multidomain: a unique computational model to study effects of a discontinuous cardiac microstructure on impulse propagation. *Biophys. J.* 95:3724–3737, 2008.

[22]Satoh, H., L. M. D. Delbridge, L. A. Blatter, and D. M. Bers. Surface:volume relationship in cardiac myocytes studied with confocal microscopy and membrane capacitance measurements: species-dependence and developmental effects. *Biophys. J.* 70:1494–1504, 1996.

[23]Shome, S., J. G. Stinstra, C. S. Henriquez, and R. S. MacLeod. Influence of extracellular potassium and reduced extracellular space on conduction velocity during acute ischemia: a simulation study. *J. Electrocardiol.* 39:S84–S85, 2006.

[24]Sommer, J. R., and E. A. Johnson. Ultrastructure of cardiac muscle. In: Handbook of Physiology, Section 2: The Cardiovascular System, Vol. 1. American Physiological Society, 1979, pp. 113–186.

[25]Spach, M. S. Microfibrosis produces electrical load variations due to loss of side-to-side cell connections. *PACE* 20:397–413, 1997.

[26]Spach, M. S., J. F. Heidlage, E. R. Darken, E. Hofer, K. H. Raines, and C. F. Starmer. Cellular dvmax/dt reflects both membrane properties and the load presented by adjoining cells. *Am. J. Physiol. (Heart Circ. Physiol.)* 32:H1855–H1863, 1992.

[27]Stinstra, J. G., B. Hopenfeld, and R. S. MacLeod. On the passive cardiac conductivity. *Ann. Biomed. Eng.* 33(12): 1743–1751, 2005.

[28]Stinstra, J. G., S. Roberts, J. Pormann, R. S. MacLeod, and C. S. Henriquez. A model of 3d propagation in discrete cardiac tissue. *Comput. Cardiol.* 33:41–44, 2006.

[29]Stinstra, J. G., S. Shome, B. Hopenfeld, and R. S. MacLeod. Modeling the passive cardiac electrical conductivity during ischemia. *Med. Biol. Eng. Comput.* 43(6):776–782, 2005.

[30]Trautman, E. D., and R. S. Newbower. A practical analysis of the electrical conductivity of blood. *IEEE Trans. Biomed. Eng.* 30(3):141–153, 1983.

[31]Trayanova, N., G. Plank, and B. Rodriguez. What have we learned from mathematical models of defibrillation and postshock arrythmogenesis? Application of bidomain simulations. *Heart Rhythm* 3(10):1232–1235, 2006.